Wintertime ocean–atmosphere interaction processes associated with the SST variability in the North Pacific subarctic frontal zone

Qionghui Huang[1] · Jiabei Fang[1,2] · Lingfeng Tao[1] · Xiu-Qun Yang[1]

Abstract

Recent research indicates that the midlatitude oceanic frontal zones are the key regions of ocean–atmosphere interaction. The thermal condition of midlatitude ocean in frontal zones can affect the atmosphere efficiently through both diabatic heating and transient eddy feedback. In this study, the wintertime SST variability in the subarctic frontal zone (SAFZ) of the North Pacific and the associated ocean–atmosphere interaction mechanism are examined based on observational and theoretical analyses. It is found that the SAFZ-related SST anomaly is characterized as a large-scale interannual mode that can persist during the whole winter, and that its evolution is accompanied with local ocean–atmosphere interaction processes. The initial anticyclonic surface wind anomaly associated with the weakened Aleutian Low forces a large-scale warm SST anomaly in midlatitude North Pacific by driving northward Ekman flow and downward heat flux. With the increase of SST anomaly, the air-sea heat flux exchange reverses, indicating that the ocean starts to heat the atmosphere. In addition to increasing the diabatic heating, the warm SST anomaly strengthens the SST gradient in the north part of SAFZ. The low-level atmospheric baroclinicity is adjusted to synchronize with the SAFZ correspondingly due to oceanic thermal influence, causing change of transient eddy activities. Though all the ocean-induced diabatic heating, transient eddy heating and transient eddy vorticity forcing are enhanced over SAFZ, the last physical process plays the most important role in shifting and maintaining the equivalent barotropic atmospheric circulation anomalies. Therefore, the ocean–atmosphere interaction provides a mechanism for the development and maintenance of SAFZ-related anomalies of the North Pacific ocean–atmosphere system throughout the winter.

Keywords Midlatitude ocean–atmosphere interaction · North Pacific · Subarctic frontal zone · Transient eddy feedback · Wintertime

1 Introduction

Midlatitude ocean–atmosphere interaction is widely considered to be an important source of decadal to interdecadal climate variability (Nakamura et al. 1997; Pierce et al. 2001; Zhong et al. 2008; Kelly et al. 2010; Kwon et al. 2010; Liu and Di Lorenzo 2018). However, the mechanism responsible for the midlatitude ocean–atmosphere interaction remains unclear for a long time, primarily because compared with the

✉ Jiabei Fang
fangjb@nju.edu.cn

[1] CMA-NJU Joint Laboratory for Climate Prediction Studies, School of Atmospheric Science, Nanjing University, 163 Xianlin Avenue, Nanjing 210023, China

[2] Southern Marine Science and Engineering Guangdong Laboratory (Zhuhai), Zhuhai 519082, China

strong atmospheric forcing on the ocean (Hasselmann 1976; Seager et al. 2001; Nonaka et al. 2006, 2008; Qiu et al. 2014; Yao et al. 2017), whether and in what way the midlatitude ocean affects the atmosphere have not been fully understood (Kushnir and Held 1996; Liu and Di Lorenzo 2018).

The typical dynamical structure of the midlatitude ocean–atmosphere system anomalies is different from that of the tropical ocean–atmosphere system. Corresponding to a basin-scale cold (warm) SST anomaly, the atmospheric geopotential height aloft shows a consistent low (high) anomaly in the vertical direction throughout the troposphere (Palmer and Sun 1985; Kushnir and Lau 1992; Kushnir et al. 2002; Deser et al. 2004; Fang and Yang 2016; Wang et al. 2017; Sun et al. 2018; Wills and Thompson 2018; Tao et al. 2020). This structure, also called the equivalent barotropic cold/trough (warm/ridge) structure, cannot be explained by the thermal-driven circulation theory that is applicable in

the tropics. In the middle latitudes, on one hand, the SST-induced diabatic heating is relatively weak and mainly confined to the lower troposphere due to the stable atmospheric stratification. On the other hand, the midlatitude atmosphere is strongly baroclinic, and the synoptic transient eddy activities are vigorous, featuring storm tracks (Hoskins and Valdes 1990; Chang and Orlanski 1993; Chang et al. 2002; Kushnir et al. 2002; Nakamura et al. 2004, 2008; Nakamura and Shimpo 2004; Ren et al. 2007, 2010; Small et al. 2008; Sampe et al. 2010; Chu et al. 2013; Liu et al. 2014; Okajima et al. 2022). The systematical transportations of heat, moisture and momentum by transient eddies can in turn drive and maintain the midlatitude mean atmospheric circulations (Chang and Orlanski 1993; Chang et al. 2002; Ren et al. 2010; Sampe et al. 2010; Xiang and Yang 2012; Nie et al. 2013, 2014; Fang and Yang 2016; Wang et al. 2017; Tao et al. 2020). Therefore, the midlatitude atmospheric circulation is both thermal- and transient eddy-driven, and the midlatitude SST anomalies can affect the atmosphere by changing both the diabatic heating and the transient eddy feedback (Nakamura et al. 2004, 2008; Nonaka et al. 2009; Taguchi et al. 2009, 2012; Sampe et al. 2010; Hotta and Nakamura 2011; Fang and Yang 2016; Tao et al. 2020, 2022).

In the past two decades, an increasing number of studies based on high-resolution observational data and high-resolution numerical model revealed that the midlatitude oceans can actively influence the atmosphere, especially over the oceanic frontal zones (Kushnir et al. 2002; Feliks et al. 2004, 2007, 2011; Minobe et al. 2008; Small et al. 2008; Taguchi et al. 2009; Sampe et al. 2010; Czaja and Blunt 2011; Smirnov et al. 2015; Wills and Thompson 2018; Yook et al. 2022). The midlatitude large-scale oceanic front zone is the region with the strongest SST gradient, and also associated with strongest SST variability. It not only corresponds to the intense air-sea heat exchange, but is also closely related to the atmospheric baroclinicity and transient eddy activities (Nakamura et al. 2004; Nakamura and Shimpo 2004; Nakamura and Yamane 2009, 2010; Taguchi et al. 2009; Sampe et al. 2010; Fang and Yang 2016; Tao et al. 2020). The SST variation in oceanic frontal zone, which usually shows large-scale pattern, is accompanied with the intensity change and meridional movement of the atmospheric baroclinic zone as well as the in-phase changes of the upper westerly jet and storm tracks (Nakamura et al. 2004; Nakamura and Shimpo 2004; Nakamura and Yamane 2009, 2010; Taguchi et al. 2012). Therefore, the midlatitude oceanic frontal zone is the key region of ocean–atmosphere interaction.

Our previous work Fang and Yang (2016) investigated the features and dynamics of North Pacific ocean–atmosphere anomalies associated with the Pacific Decadal Oscillation (PDO). Based on observational study and quantitative dynamical diagnosis, a positive feedback mechanism for midlatitude unstable air-sea interaction in the North Pacific was hypothesized. In the hypothesis, the PDO-related SST anomaly is mainly forced by the surface heat flux and Ekman current advection induced by anomalous atmospheric westerly. Then, the basin-scale SST anomaly tends to change the direction of air-sea heat flux exchange and the intensity of the subtropical oceanic front of North Pacific, resulting in the anomalies of both diabatic heating and transient eddy thermal and dynamical forcing. The transient eddy dynamical forcing that dominates the total atmospheric forcing tends to produce an equivalent barotropic atmospheric circulation response that intensifies the initial surface westerly anomaly. Hence the midlatitude air-sea interaction, in which the oceanic front and atmospheric transient eddy feedback are the indispensable, can provide a positive feedback mechanism for the development and maintenance of PDO-related anomalies in the midlatitude North Pacific ocean–atmosphere system. This hypothesis has been confirmed by the later observational, theoretical and modeling studies (Wang et al. 2017; Chen et al. 2020; Tao et al. 2020, 2022; Zhang et al. 2020; Fang et al. 2022).

However, the above midlatitude ocean–atmosphere interaction mechanism is proposed based on the simultaneous correlation of seasonal-mean data that is already an equilibrium state after air-sea adjustment. The detailed interaction processes, especially the oceanic feedback process to the atmosphere, needs to be further revealed and verified from the observation. Furthermore, during the wintertime, there actually exist two oceanic frontal zones in the midlatitude North Pacific, i.e., the subtropical frontal zone (STFZ) and the subarctic frontal zone (SAFZ). The latter, formed by the convergence of warm Kuroshio current and cold Oyashio current, is much stronger than the former and could exist all the year round (Nakamura et al. 1997; Nakamura and Kazmin 2003; Wang et al. 2017). Previous studies revealed that the air-sea interaction near the SAFZ is particularly intensive over the North Pacific during the winter (Nakamura et al. 2008; Sampe et al. 2010; Frankignoul et al. 2011; Yao et al. 2017, 2018; Wills and Thompson 2018). The cross-frontal differential heat flux in SAFZ effectively offsets the relaxing effect of transient eddies, acting to maintain the near-surface baroclinicity and anchor the storm track, which is called the oceanic baroclinic adjustment mechanism (Nakamura et al. 2008; Sampe et al. 2010). Frankignoul et al. (2011) found the SST anomaly in SAFZ could excite downstream curl response in the eastern North Pacific, which causes subsequent westward-propagating Rossby waves impacting the whole gyre circulation. However, what are the evolution characteristics of the ocean–atmosphere system anomalies associated with the SAFZ during the winter, how does the midlatitude ocean–atmosphere interaction contribute to them, and what are the specific physical processes of ocean–atmosphere

interaction? These issues remain to be further explored based on observational study.

In the present study, we focus on the anomalies of the North Pacific ocean–atmosphere system associated with SAFZ variability during the wintertime. A lead-lag regression analysis with high-resolution data is applied to identify the evolution characteristics of the SAFZ-related air-sea anomalies. Based on the diagnoses of the oceanic mixed-layer temperature tendency equation and the atmospheric quasi-geostrophic potential vorticity (QGPV) equation, the ocean–atmosphere interaction processes and their roles in the development and evolution of the air-sea anomalies are examined. It is found that the unstable ocean–atmosphere interaction mechanism proposed by Fang and Yang (2016) also works in the issues we discuss. It helps to maintain the atmospheric anomalies throughout the winter season.

The manuscript is organized as follows. Section 2 introduces the data and methods. Evolution characteristics of the air-sea variable anomalies associated with the SAFZ are investigated in Sect. 3. The corresponding ocean–atmosphere interaction processes are explored in Sect. 4. Section 5 is devoted to the conclusions and discussion.

2 Data and methods

The analyzed data used in the present study are from the European Centre for Medium-Range Weather Forecasts (ECMWF) ERA5 hourly reanalysis products, with a horizontal resolution of 0.25° longitude × 0.25° latitude. The surface variables include sea surface temperature (SST), sea level pressure (SLP), sensible heat flux (SHF) and latent heat flux (LHF) (positive denoting upward). The multi-level variables include geopotential height (hereafter denoted by Z), air temperature, wind field and relative vorticity from 100 to 1000 hPa. Other oceanic data including sea water potential temperature, potential density, velocity, mixed-layer depth (MLD), and wind stress are from the Simple Ocean Data Assimilation (SODA) version 3.4.2 5-day reanalysis products (Carton et al. 2018), with a spatial resolution of 0.5° longitude × 0.5° latitude. In our study, the hourly ERA5 data has been processed into daily-mean, and the SODA data has also been interpolated into daily data before analysis. Our study focuses on the boreal winter (December–February) from 1980 to 2020, linear trend and seasonal cycle (daily climatological mean) are removed for all the data.

The atmospheric baroclinicity is represented by the maximum Eady growth rate (EGR) (Eady 1949; Lindzen and Farrell 1980) as $\sigma_{BI} = 0.3098 \cdot |f| \cdot \left|\frac{\partial u}{\partial z}\right|/N$, where f is the Coriolis parameter, u the zonal wind, and $N = \left(g\frac{\partial \ln\theta}{\partial z}\right)^{1/2}$ the *Brunt-Väisälä* frequency.

3 Evolution of the ocean–atmosphere anomalies associated with the SAFZ-SST variability

The large-scale North Pacific SAFZ refers to the belt-shaped region of strongest meridional SST gradient located around 40°N (Fig. 1a) in the northwestern Pacific. It is mainly composed by the western boundary warm Kuroshio current at 35°N, the cold Oyashio current at about 40°N, and their eastward extension areas. In the wintertime North Pacific, SAFZ is also the region of strongest SST variability (Fig. 1b), and it corresponds to intense upward heat flux transport from the ocean (Fig. 1c). The atmospheric circulation over the North Pacific is characterized by deep westerly jet stream with its maximum value at about 200 hPa (Fig. 5a). The jet core locates near 32°N, south of the SAFZ, and the corresponding surface Aleutian Low (AL) lies north of the SAFZ (Fig. 1d). Accompanied by the westerly jet, the midlatitude atmosphere shows strong baroclinicity (Fig. 5b), and the synoptic transient eddies stimulated by baroclinic instability develop vigorously, favoring North Pacific storm track. The core of the storm track in the lower troposphere and the poleward transient eddy heat transport are highly correlated to the strong oceanic front (Fig. 1e). Previous researches based on global climate model (GCM) numerical simulations (Nonaka et al. 2009; Taguchi et al. 2009; Sampe et al. 2010) have suggested that the heat supply from the ocean around the frontal zone helps to maintain an atmospheric baroclinic zone and thereby acts to anchor a storm track.

To demonstrate the SST variability associated with the SAFZ, we define an index by averaging the wintertime (DJF) SST anomaly within the region of 37.5°–44.5°N, 144°–172°E (Fig. 2a), hereafter called the SAFZ-SST index. The SAFZ-SST index is standardized and a 7-day running mean is performed to remove the synoptic disturbance. The regressed SST anomaly displays a large-scale pattern with a warming anomaly in the western-to-central midlatitude North Pacific and a surrounding cooling anomaly along the west coast of North America continent and in the subtropical North Pacific (Fig. 2b). Resultantly, the meridional SST gradient on the north (south) side of SAFZ increases (decreases) (Fig. 2b), conductive to the poleward displacement of SAFZ. Such SAFZ-related SST variability is an interannual mode with a main period of about 2–3 years, but it shows insignificant correlation with ENSO ($r = 0.0374$) (Nakamura et al. 1997; Nakamura and Yamagata 1999; Frankignoul et al. 2011; Wills and Thompson 2018), representing an independent midlatitude oceanic mode of the North Pacific.

Figure 3 exhibits the lead-lag regression of SST, surface turbulent heat flux (THF, sum of SHF and LHF), SLP
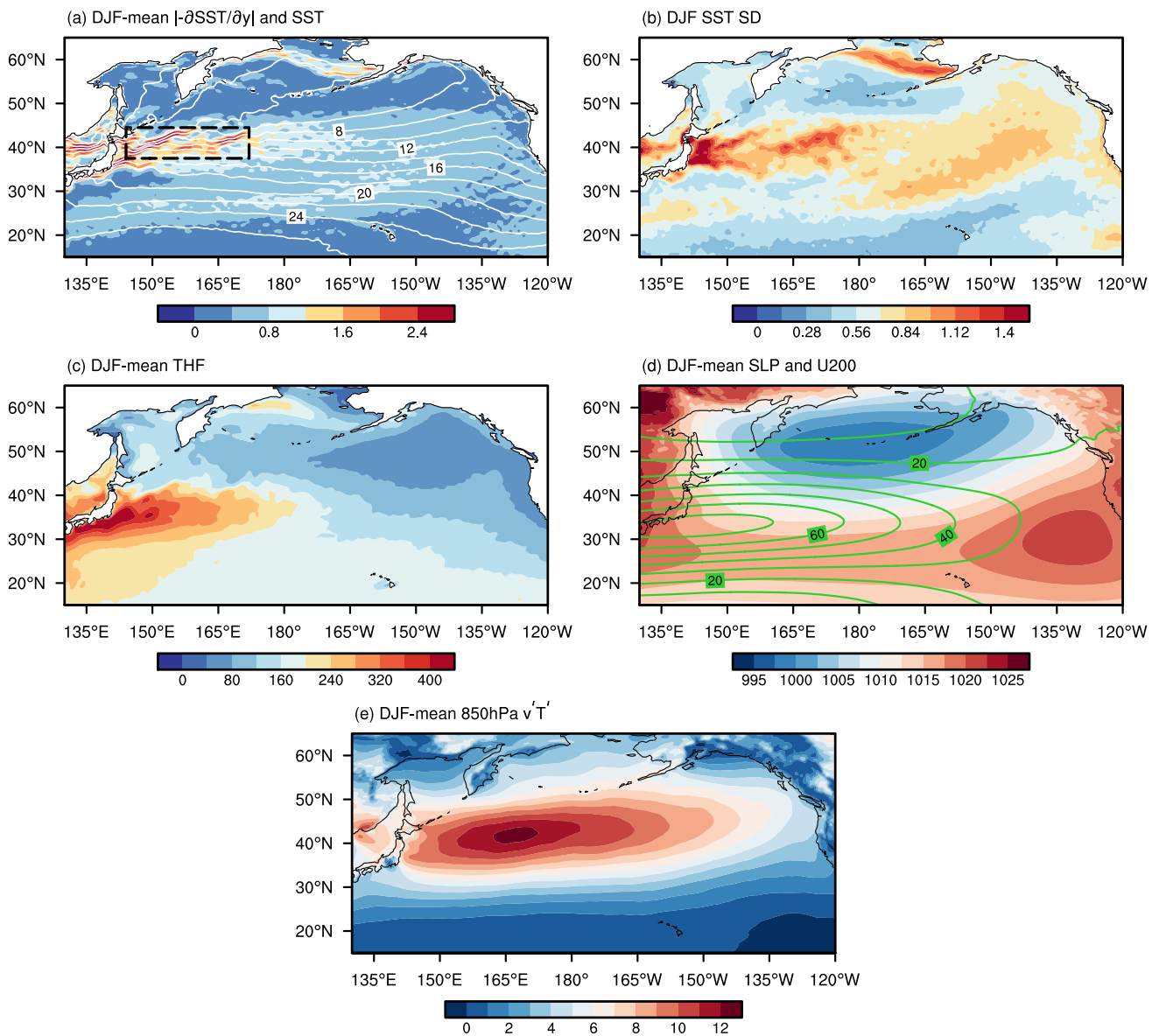
Fig. 1 Wintertime (DJF) climatological mean states of **a** SST (℃; contours) and its meridional gradient (10^{-5} ℃/m; shaded), **b** standard deviation (SD) of SST, **c** turbulent heat flux (THF; W/m^2; positive denoting upward), **d** SLP (hPa; shaded) and the zonal wind at 200 hPa (U200; m/s; contours; positive denoting westerly), and **e** meridional transient eddy heat flux (℃·m/s). The dashed box in (**a**) refers to the region of 37.5°–44.5°N, 144°–172°E for the definition of SAFZ-SST index

and Z200 anomalies onto the SAFZ-SST index during the wintertime. Note that in the present study, we use "leading phase" ("lagging phase") to denote the time when regressed variables lead (lag) the SAFZ-SST index. The specific days for variables leading or lagging the SAFZ-SST index are shown on the right side of the panel. For example, "− 30 days" ("+ 30 days") on the right side of the panel (Fig. 3) denotes regressed anomalies leading (lagging) the SAFZ-SST index by 30 days. As shown by Fig. 3a–f, the SST anomaly is prominent and persistent during the whole winter season. It enhances in the leading

phase, reaches the maximum at 0 day, and weakens gradually in the lagging phase.

However, the associated THF anomaly undergoes a phase reversal (Fig. 3g–l). In the leading phase, the warm SST anomaly corresponds to a downward THF anomaly in the SAFZ (Fig. 3g–h), while in the lagging phase, the warm SST anomaly is related to an upward THF anomaly (Fig. 3j–l). The relative contributions of oceanic and atmospheric anomalies to the anomalous THF can be quantified based on the decomposition of bulk formulas (see Appendix). It is illustrated that the downward heat flux anomaly in the
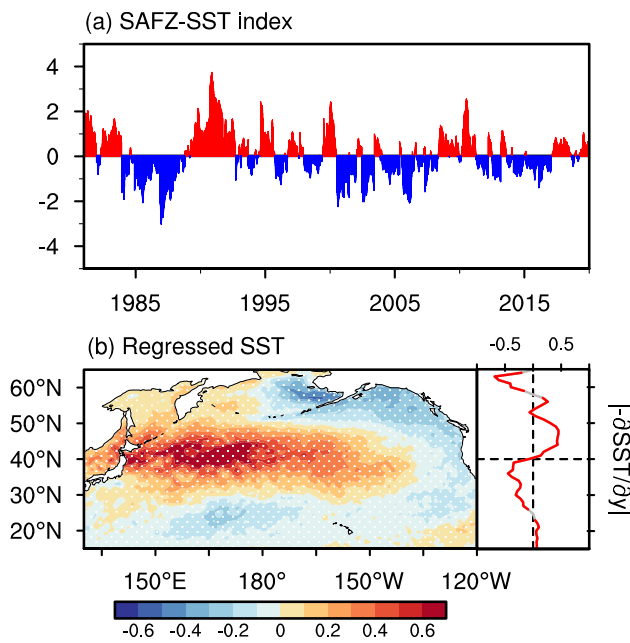
(a) SAFZ-SST index

(b) Regressed SST

Fig. 2 Definition of the wintertime (DJF) SAFZ-SST index. **a** SAFZ-SST index defined by averaging the SST anomalies within the region indicated by the dashed box in Fig. 1a (i.e., 37.5°–44.5°N, 144°–172°E). The index is standardized and a 7-day running mean is applied to remove the synoptic disturbance. **b** Simultaneous regression of SST (℃) onto the SAFZ-SST index, with corresponding zonal mean meridional gradient of SST (10^{-6} ℃/m) within 144°–172°E attached on the right side. Stippling in shaded and red color in line indicate statistical significance at the 95% confidence level based on the two-tailed Student's *t* test. The effective degrees of freedom are calculated after Bretherton et al. (1999)

leading phase is dominated by the atmospheric anomalies while the upward heat flux anomaly in the lagging phase is determined by the SST anomaly. Hence, the change of relationship between SST anomaly and THF anomaly suggests that the atmosphere forces the ocean in the leading phase while the ocean turns to force the atmosphere in the lagging phase.

The corresponding atmospheric circulation anomalies also show obvious variation during the wintertime. There is a strong positive SLP anomaly to the north of 40°N, indicating a weakened AL, and a week negative SLP anomaly in its south in the leading phase (Fig. 3m–n). The positive anomaly peaks at about − 15 day, then decays rapidly and retreats to the north after 0 day. Meanwhile, the negative SLP anomaly is enhanced and moves northward with two centers located in the western and eastern midlatitude North Pacific respectively (Fig. 3p). It should be noted that the positive SLP anomaly is strengthened again at + 45 day after being largely reduced, and the negative anomaly moves eastward, forming a dipole structure (Fig. 3q–r). Similar characteristics can be also found in the evolution of Z200 anomalies (Fig. 3s–x), which confirm the equivalent barotropic

structure in the vertical direction of midlatitude atmospheric anomalies.

Clues of ocean–atmosphere interaction can be found in the evolution of oceanic and atmospheric anomalies associated with the SAFZ-SST variability. The dominant role between ocean and atmosphere in the interaction process changes from the leading phase to the lagging phase. The ocean seems to be passive in the leading phase but later starts to force the atmosphere firstly by driving upward heat flux. Then, what cause the changes of SST anomalies and atmospheric anomalies, and how the ocean feedbacks on the atmosphere, especially why the atmospheric anomaly is re-enhanced, will be analyzed in detail below.

4 Ocean–atmosphere interaction processes associated with the SAFZ-SST variability

Here we diagnose the oceanic mixed-layer temperature tendency equation and the atmospheric QGPV equation respectively to further understand the mechanism of ocean–atmosphere interaction during the evolution process.

4.1 Mechanism responsible for the variation of SST anomalies

Following Qiu (2000) and Yao et al. (2017), the mixed-layer temperature tendency equation can be written as

$$\frac{\partial T}{\partial t} = \frac{Q_{net}}{\rho c_p h} - \vec{V}_{ek} \cdot \nabla T - \frac{w_e|_{z=-h}(T - T|_{z=-h})}{h}, \tag{1}$$

where T denotes the mixed-layer temperature, ρ the sea water density, c_p the specific heat capacity of sea water, h the MLD, Q_{net} the net surface turbulent heat flux, $\vec{V}_{ek}$ the Ekman advection velocity, and w_e the vertical entrainment velocity. According to the equation, three types of physical processes can lead to the change of SST, i.e., the net surface turbulent heat flux, the horizontal Ekman advection driven by surface wind stress, and the vertical entrainment. Note that the advection of geostrophic flow, which is proven to be unimportant by previous studies (Fang and Yang 2016; Yao et al. 2017; Tao et al. 2022), has been neglected in the equation.

Figure 4 shows the evolution of SST tendencies induced by the three terms, respectively. The THF-induced SST anomaly in SAFZ also reverses between leading and lagging phases (Fig. 4a–f), similar as the THF anomaly (Fig. 3g–l). In the leading phase, the heat is transported from the atmosphere to the ocean over SAFZ region (Fig. 3g–h), and thus the SST tends to be increased there (Fig. 4a–b). When the ocean is warmer than the atmosphere at the air-sea interface, the ocean starts to heat the atmosphere in turn (Fig. 3j–l).
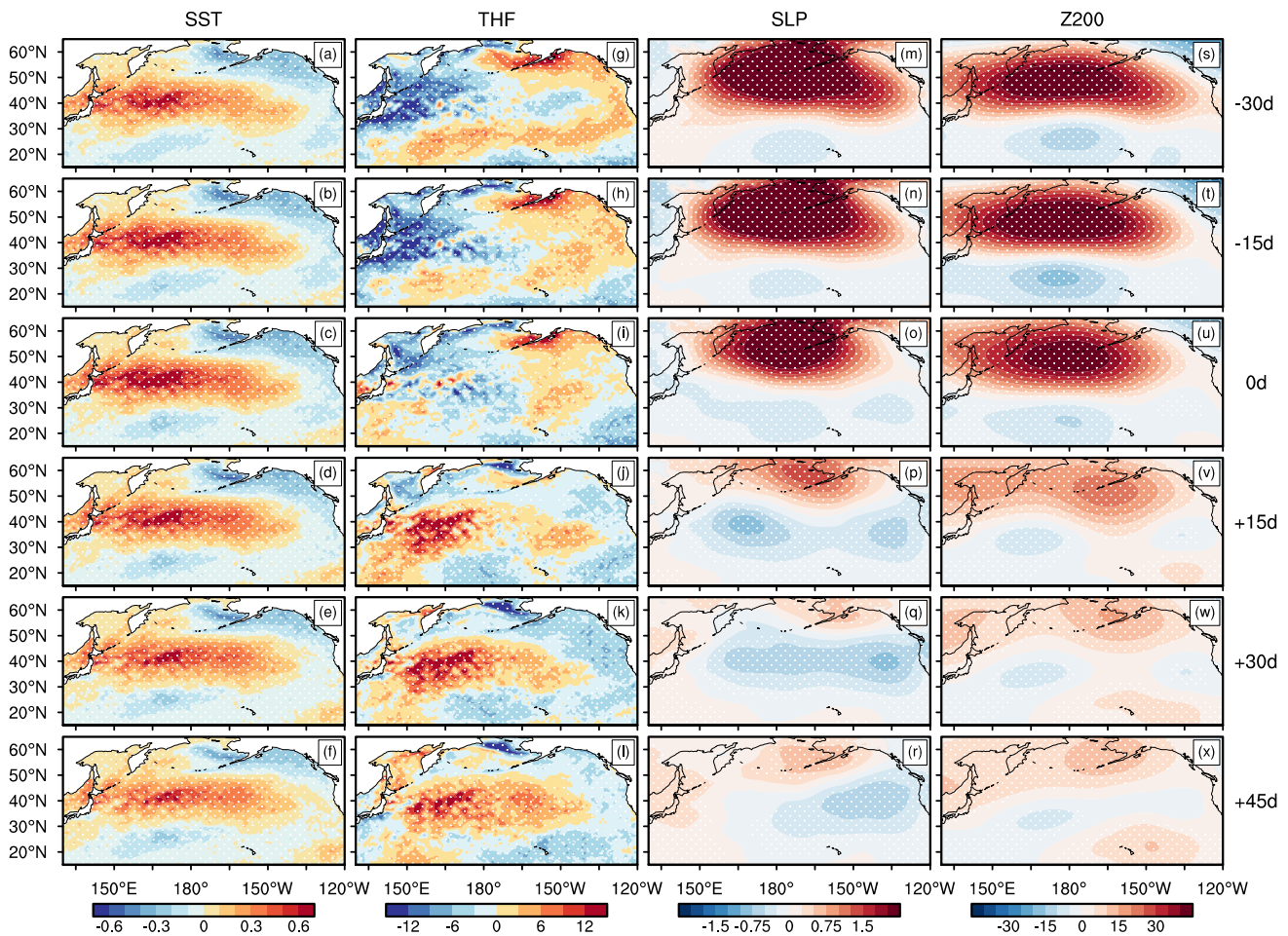
Fig. 3 Lead-lag regression of **a–f** SST (℃), **g–l** THF (W/m²), **m–r** SLP (hPa), and **s–x** geopotential height at 200 hPa (Z200; **m**) onto the SAFZ-SST index. Negative (positive) number on the right side denotes the number of days leading (lagging) the SAFZ-SST index. Stippling indicates statistical significance at the 95% confidence level based on the two-tailed Student's *t* test

So in the lagging phase, the SST in SAFZ is decreased due to heat release to the atmosphere (Fig. 4d–f). On the other hand, the westward wind stress on the south side of the positive SLP anomaly can drive northward oceanic Ekman flow. They transport warm water to the midlatitude North Pacific, leading to warm SST anomaly there (Fig. 4g–i). However, SST anomaly induced by the Ekman advection anomaly is strong in the leading phase, but greatly abates in the lagging phase (Fig. 4j–l), consistent with the evolution of SLP anomaly (Fig. 3m–r). By contrast, the wind-driven vertical entrainment always reduces the SST anomaly in the western-to-central North Pacific, but its influence on SST anomaly is always small and can be ignored (Fig. 4m–r).

Through the diagnosis of mixed-layer temperature tendency equation, we can find that the Ekman advection dominates the total forcing term in the leading phase and its distribution pattern is similar as that of the SST anomaly. At this time, the atmosphere forces the upper ocean mainly by driving Ekman advection, and the warm SST anomaly

increases. While in the lagging phase, the ocean turns to feedback on the atmosphere, and the ocean-induced upward heat flux damps SST itself gradually.

4.2 Mechanism responsible for the variation of atmospheric circulation anomalies

The midlatitude atmosphere follows quasi-geostrophic dynamics. Following Fang and Yang (2016), the time-mean atmospheric QGPV equation can be written as

$$
\left(\frac{\partial}{\partial t} + \overrightarrow{V_h} \cdot \nabla \right) \left[\frac{1}{f}\nabla^2\overline{\phi} + f + \frac{\partial}{\partial p}\left(\frac{f}{\overline{\sigma}_1}\frac{\partial \overline{\phi}}{\partial p} \right) \right]
$$
$$
= \underbrace{-f\frac{\partial}{\partial p}\left(\frac{\overline{\alpha}}{\overline{\sigma}_1}\frac{\overline{Q}_d}{\overline{T}} \right)}_{F_1} \underbrace{-f\frac{\partial}{\partial p}\left(\frac{\overline{\alpha}}{\overline{\sigma}_1}\frac{\overline{Q}_{eddy}}{\overline{T}} \right)}_{F_2} + \underbrace{\overline{F}_{eddy}}_{F_3}, \quad (2)
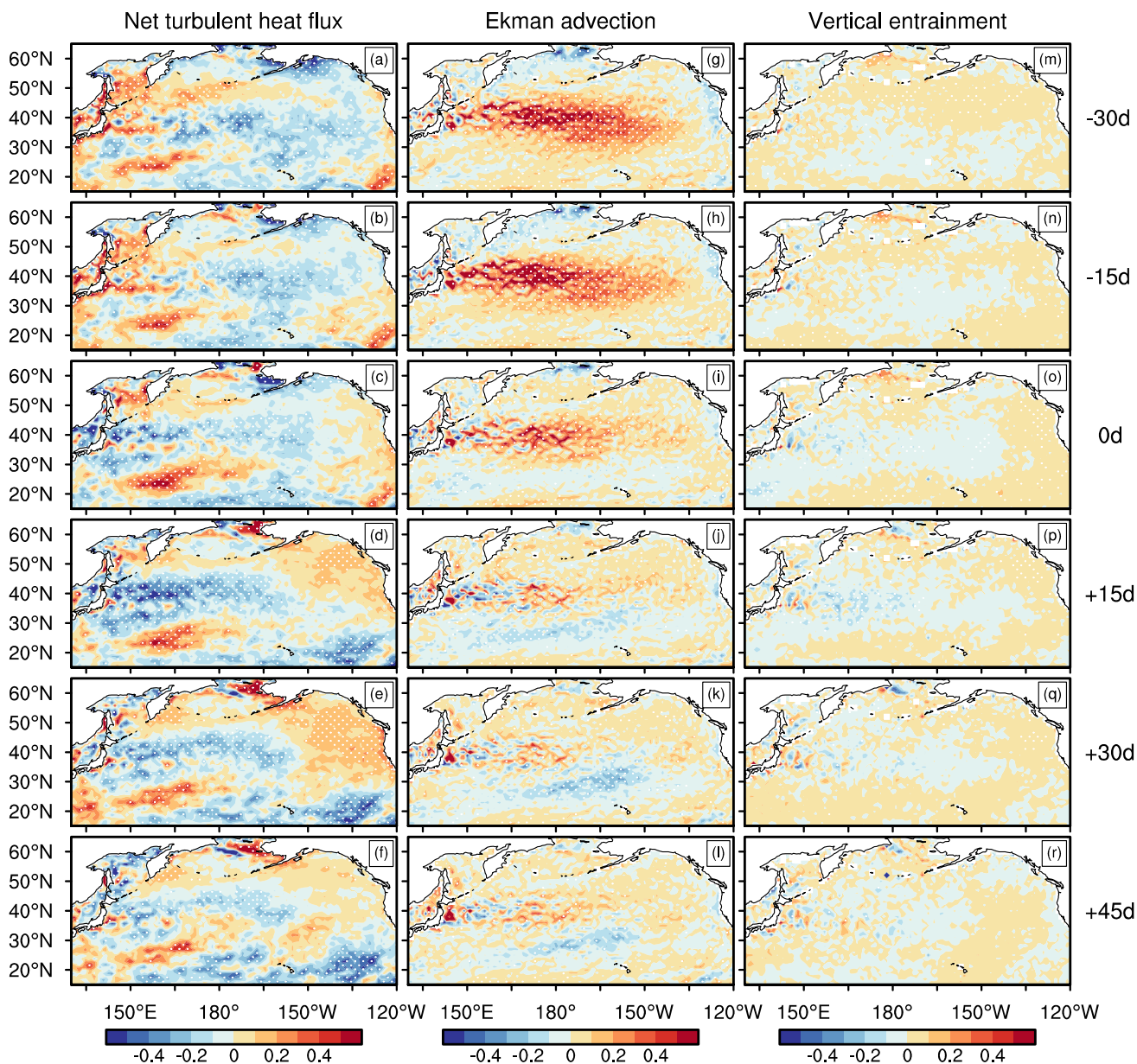$$

Fig. 4 As Fig. 3, but for the SST tendencies (10^{-7} °C/s) induced by (**a–f**) net turbulent heat flux, **g–l** Ekman advection, and **m–r** vertical entrainment, respectively

where the overbar denotes the time mean (7-day mean is used in this study), V_h is the geostrophic wind, ϕ the geopotential, T the air temperature, α the specific volume, and σ_1 the static stability parameter. $\overline{Q}_d$ is the time-mean diabatic heating that can be diagnosed as the residual of the thermodynamic equation (Christy 1991; Yanai and Tomita 1998), $\overline{Q}_{eddy} = -\nabla \cdot \overrightarrow{V'_h T'} - \frac{\partial \overline{\omega' T'}}{\partial p} + \frac{R}{c_p p}\overline{\omega' T'}$ and $\overline{F}_{eddy} = -\nabla \cdot \overrightarrow{V'_h \zeta'}$ are defined as the time-mean transient eddy heating and transient eddy vorticity forcing, which are caused by the

convergence of heat and vorticity flux transports by transient eddies, respectively. The frictional dissipation term has been omitted. From the perspective of QGPV dynamics, there are three PV forcing sources that can change the time-mean atmospheric circulation: the diabatic heat forcing (F_1), the transient eddy heat forcing (F_2), and the transient eddy vorticity forcing (F_3). The latter two terms represent the transient eddy thermal and dynamical feedback on the mean flow, respectively.
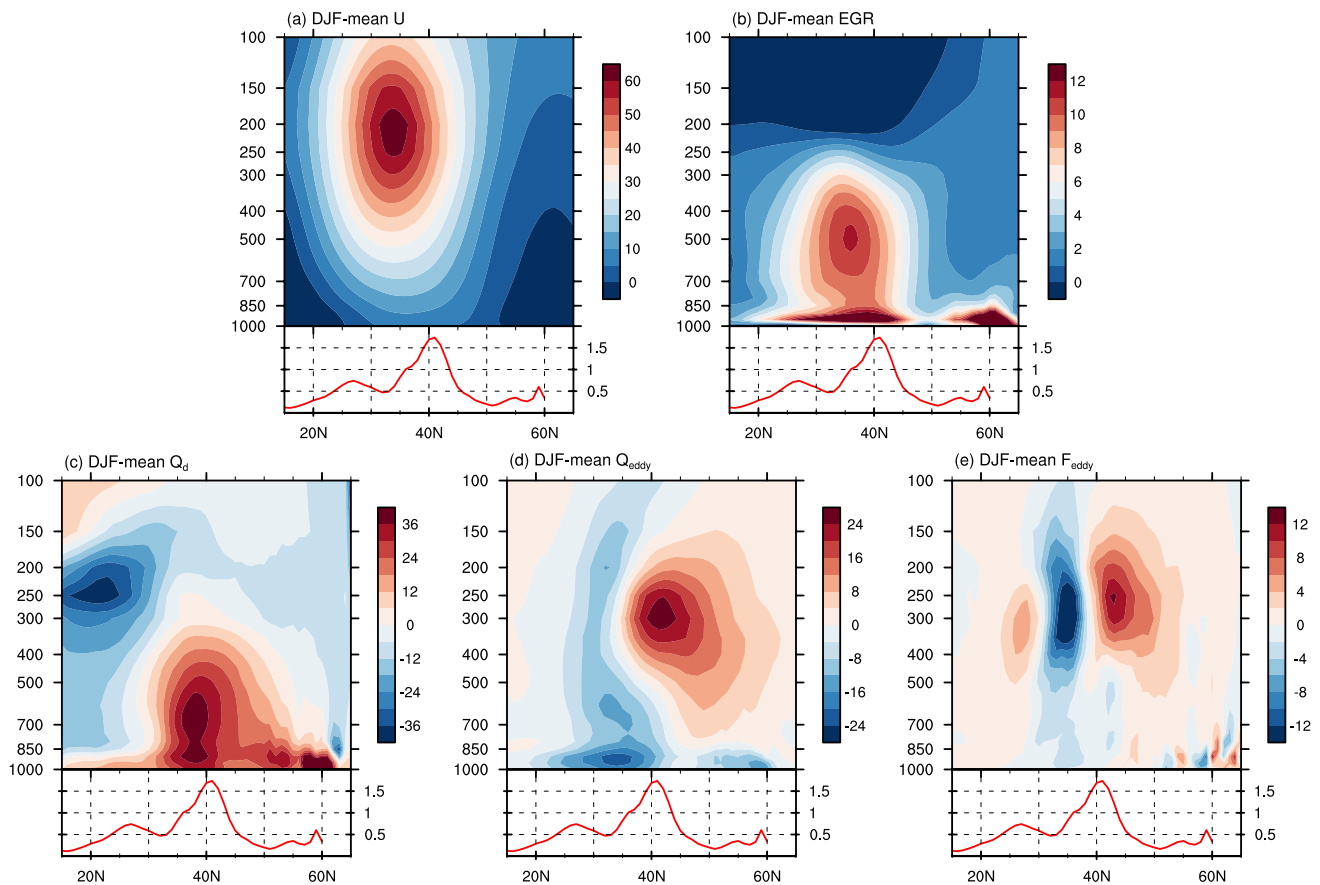
Fig. 5 Latitude-altitude sections of the wintertime (DJF) climatological mean states of **a** zonal wind ($\overline{U}$; m/s), **b** Eady growth rate (EGR; 10^{-5} $\underline{s}^{-1}$), **c** diabatic heating ($\overline{Q}_d$; 10^{-6} K/s), **d** transient eddy heating ($\overline{Q}_{eddy}$; 10^{-6} K/s), and **e** transient eddy vorticity forcing ($\overline{F}_{eddy}$; 10^{-11} s^{-2}), which are averaged between 150°E and 170°W. Corresponding zonal mean meridional gradient of SST (10^{-5} °C/m; red line) is attached in the lower panel of (**a**–**e**)

Wintertime climatological mean states of the three PV sources as well as the zonal wind (U) and EGR averaged between 150°E and 170°W are shown in Fig. 5. As we mentioned before, the ocean–atmosphere heat exchange is strong over oceanic frontal zones, and the ocean always heats the atmosphere in winter on average. However, the $\overline{Q}_d$ is relatively weak compared with that in tropics (Zhang et al. 2012) and is confined to the middle-to-lower troposphere with a maximum at 700 hPa (Fig. 5c). Meanwhile, the transient eddies that generate in the region of large atmospheric baroclinicity transport heat and vorticity flux northward systematically. The transient eddy heat and vorticity flux both converge north of the SAFZ, producing positive $\overline{Q}_{eddy}$ and $\overline{F}_{eddy}$ with maxima at 250–300 hPa (Fig. 5d, e). $\overline{Q}_{eddy}$ offsets $\overline{Q}_d$ to some extent and $\overline{F}_{eddy}$ maintains the eddy-driven westerly jet at around 40°N. Our previous works (Fang and Yang 2016; Wang et al. 2017; Tao et al. 2020) have proved that $\overline{F}_{eddy}$ plays the dominant role in the generation and maintenance of the equivalent barotropic atmospheric geopotential anomaly.

Using the successive over-relaxation (SOR) method, we can numerically solve Eq. 2 to obtain the geopotential tendencies ($\frac{\partial \overline{\phi}}{\partial t}$) induced by the three PV forcing terms, respectively (Lau and Holopainen 1984), which denote the initial atmospheric responses to the forcing terms. The lead-lag evolutions of the anomalies of $\overline{Q}_d$, $\overline{Q}_{eddy}$ and $\overline{F}_{eddy}$ (Fig. 6 and continued) as well as their causing geopotential tendencies (Fig. 7 and continued) further reveal their different roles in influencing the atmosphere. Consistent with the evolutions in Fig. 3m–x, the regressed Z anomalies develop and peak at about-15 day, then start to decay and largely weaken in lagging phase whereas enhance again at+40–45 days (Fig. 6a–d).

It can be proved that during the whole evolution process, the change of Z is determined by the three forcing terms to a great extent while the effects of advection and diffusion are secondary (Lau and Holopainen 1984). In the leading phase, since the atmosphere heats the ocean over SAFZ region, the $\overline{Q}_d$ anomaly is negative in the lower level (Fig. 6e–g). It tends to induce geopotential low anomaly below 400 hPa and thus acts to reduce the positive Z anomaly in lower
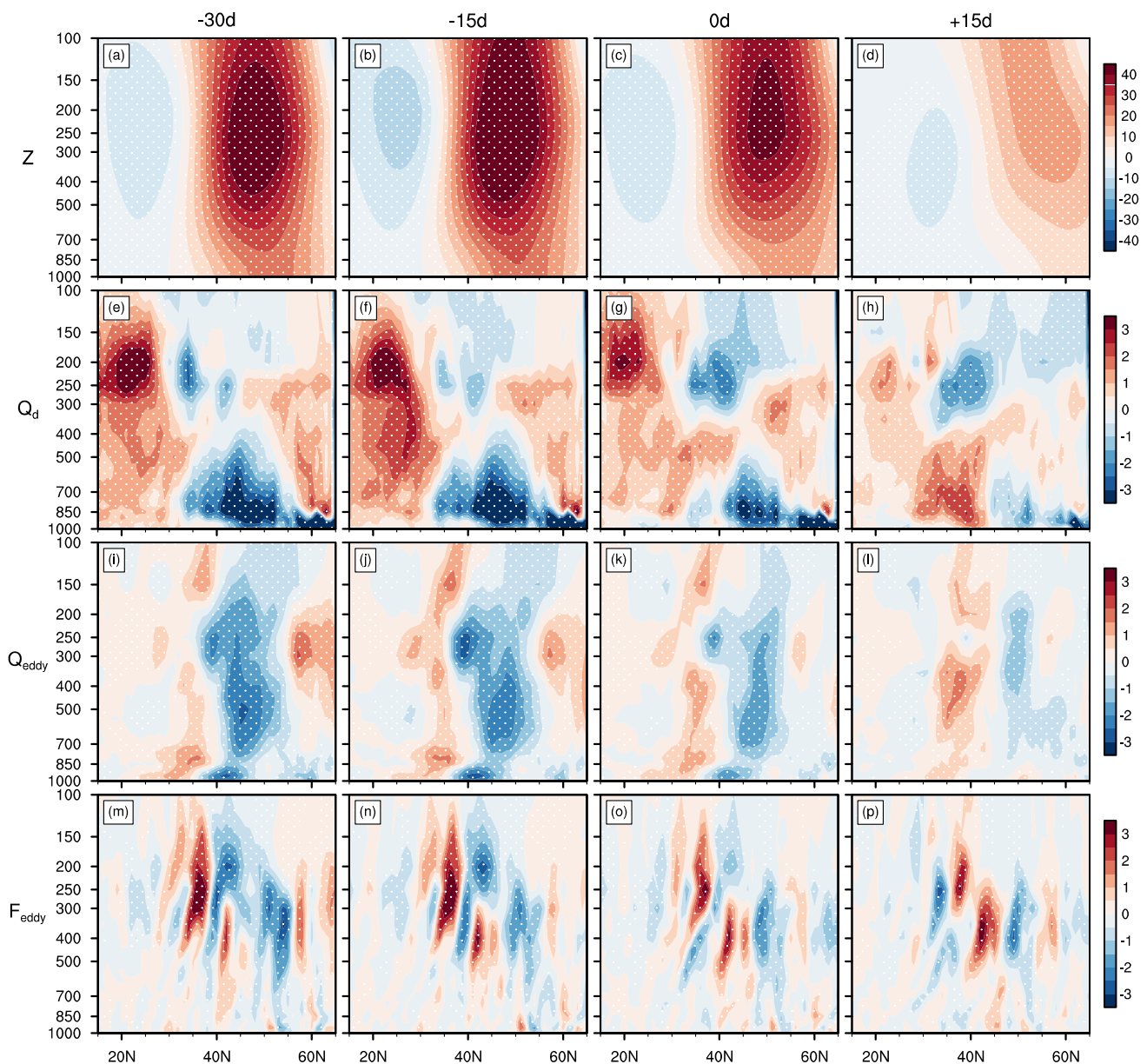
Fig. 6 Latitude-altitude sections of the wintertime (DJF) lead-lag regression of **a–d** geopotential height (Z; m), **e–h** diabatic heating ($\overline{Q}_d$; 10^{-6} K/s), **i–l** transient eddy heating ($\overline{Q}_{eddy}$; 10^{-6} K/s), and **m–p** transient eddy vorticity forcing ($\overline{F}_{eddy}$; 10^{-11} s^{-2}) upon the SAFZ-SST index, which are averaged between 150°E and 170°W. Negative (positive) number on the top of panel denotes the number of days leading (lagging) the SAFZ-SST index. Stippling indicates statistical significance at the 95% confidence level based on the two-tailed Student's t test. As in this figure, but for the lag regression from +30 day to +45 day (at 5-day interval)

troposphere (Fig. 7e–g). Meanwhile, the atmospheric baroclinicity is significantly decreased in the baroclinicity zone and SAFZ (violet lines in Fig. 8a–c). Therefore, the transient eddy activities are suppressed and both the $\overline{Q}_{eddy}$ and $\overline{F}_{eddy}$ are decreased over SAFZ (Fig. 6i–k, m–o). However, the atmospheric response to $\overline{Q}_{eddy}$ anomaly shows a geopotential low anomaly in the middle-to-upper troposphere (Fig. 7i–k), which also damps the positive Z anomaly as $\overline{Q}_d$ does. In contrast, the $\overline{F}_{eddy}$ anomaly tends to produce equivalent

barotropic atmospheric response with a geopotential high anomaly north of 40°N and a geopotential low anomaly south of 40°N (Fig. 7m–o), acting to maintain the initial atmospheric circulation anomaly.

Taken overall, the contribution of thermal forcing, including the diabatic heat forcing and the transient eddy heat forcing, exceeds that of the dynamic forcing, and thus leads to the damping of Z anomaly after-15 day (Fig. 7). It should be noted that the change of atmospheric baroclinicity in the
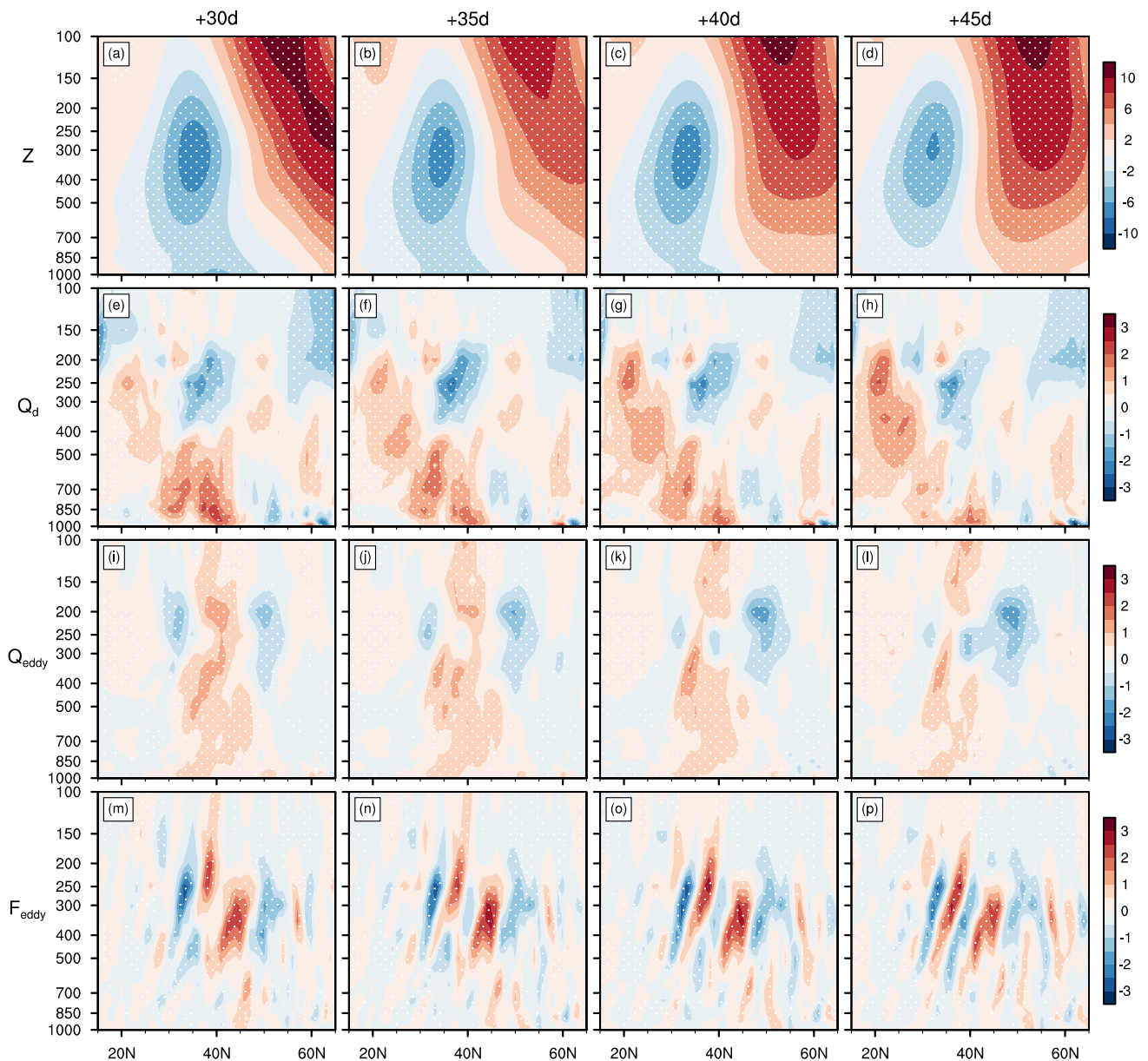
Fig. 6 (continued)

leading phase doesn't match well with that of the SST gradient (Fig. 8a–c), indicating that the transient eddy feedback is also mostly determined by the atmospheric process. Therefore, the atmosphere plays a dominant role in the leading phase and results in a self-damping effect.

When it comes to the lagging phase, the warm upper ocean in SAFZ region starts to stimulate upward heat flux anomaly (Fig. 3j–l), and the $\overline{Q}_d$ anomaly also reverses from negative to positive in the lower atmosphere (Fig. 6h and continued e–h). Influenced by the oceanic thermal forcing, the atmospheric baroclinic zone begins to be synchronized with the SAFZ, i.e., the low-level atmospheric baroclinicity increases in the north of SAFZ while weakly decreases

in the south (Fig. 8d–h). Compared to the leading phase, the positive baroclinicity region originally in the north of SAFZ moves southward and occupies above the SAFZ. At this time, the changes of atmospheric baroclinicity and the associated transient eddy activities are dominated by the ocean. The enhanced atmospheric baroclinicity then leads to stronger transient eddy heat and vorticity transport, thus $\overline{Q}_{eddy}$ and $\overline{F}_{eddy}$ anomalies become to be positive over SAFZ (Fig. 6l, p and continued i–l, m–p). The atmospheric geopotential height response to $\overline{Q}_d$ anomaly always shows baroclinic structure in the vertical direction (Fig. 7h and continued e–h), and the response to $\overline{Q}_{eddy}$ anomaly, which
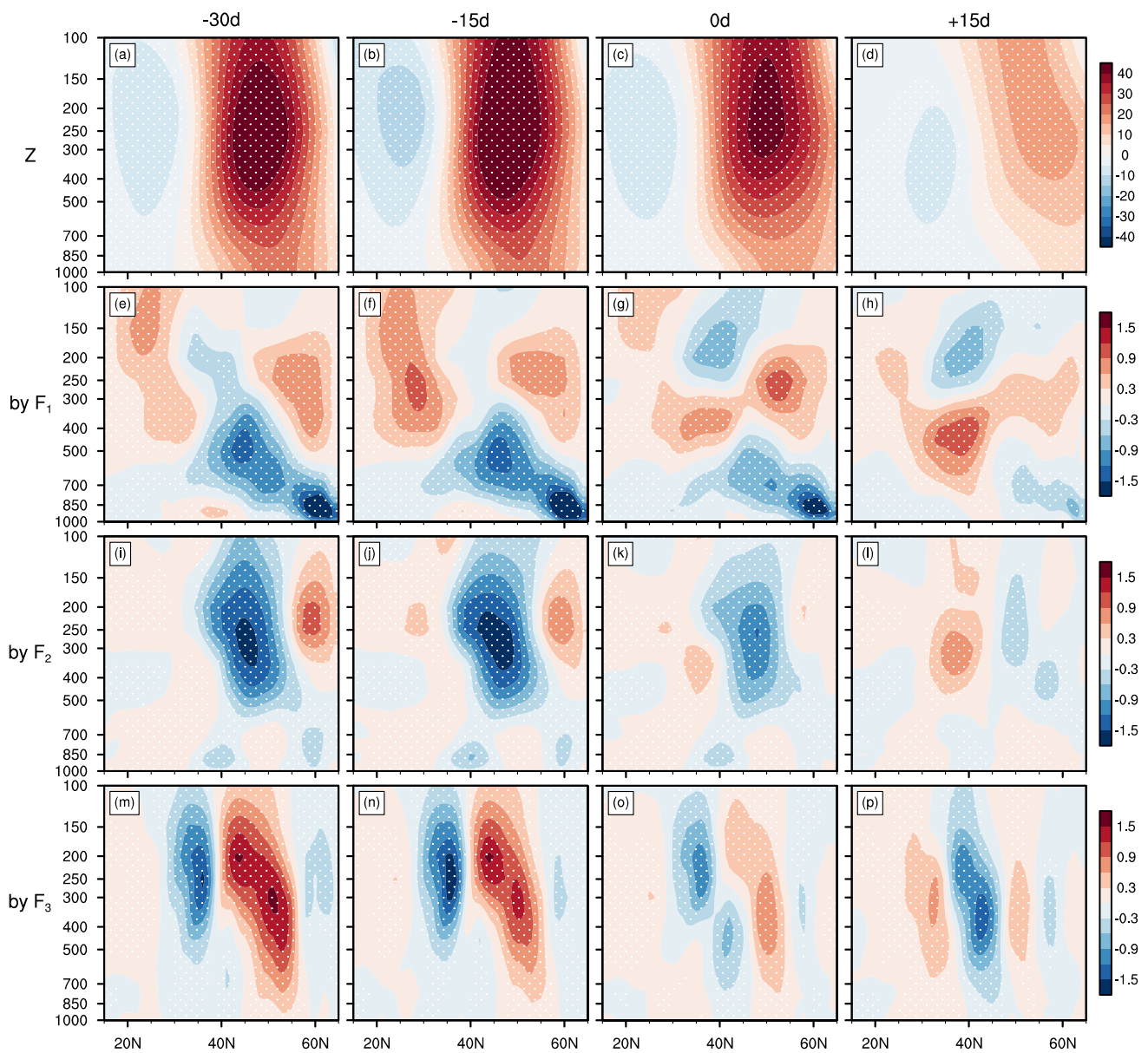
Fig. 7 As Fig. 6, but for the geopotential tendencies (10^{-4} m²/s³) induced by **e–h** diabatic heat forcing (F_1), **i–l** transient eddy heat forcing (F_2), and **m–p** transient eddy vorticity forcing (F_3), respectively. As in this figure, but for the lag regression from +30 day to +45 day (at 5-day interval)

partly cancels the contribution of $\overline{Q}_d$, always decays the Z anomaly (Fig. 7l and continued i–l). Only the $\overline{F}_{eddy}$-induced atmospheric response is equivalent barotropic (Fig. 7p and continued m–p). Its negative value around 40°N tends to cause the enhancement and northward movement of the negative Z anomaly in the south, and its positive value near 50°N helps to reinforce the positive Z anomaly in the north. Therefore, the transient eddy dynamical forcing, which dominantly contributes to the maintenance and northward shift

of the atmospheric circulation anomalies, is the main way for the ocean to affect the atmosphere in the lagging phase.

It should be pointed out that compared with the strong atmospheric forcing in the leading phase, the oceanic feedback on the atmosphere in the lagging phase is relatively weak. It takes approximately a month for the oceanic influence to be identified visibly by the re-enhancement of Z anomalies at +40–45 days.
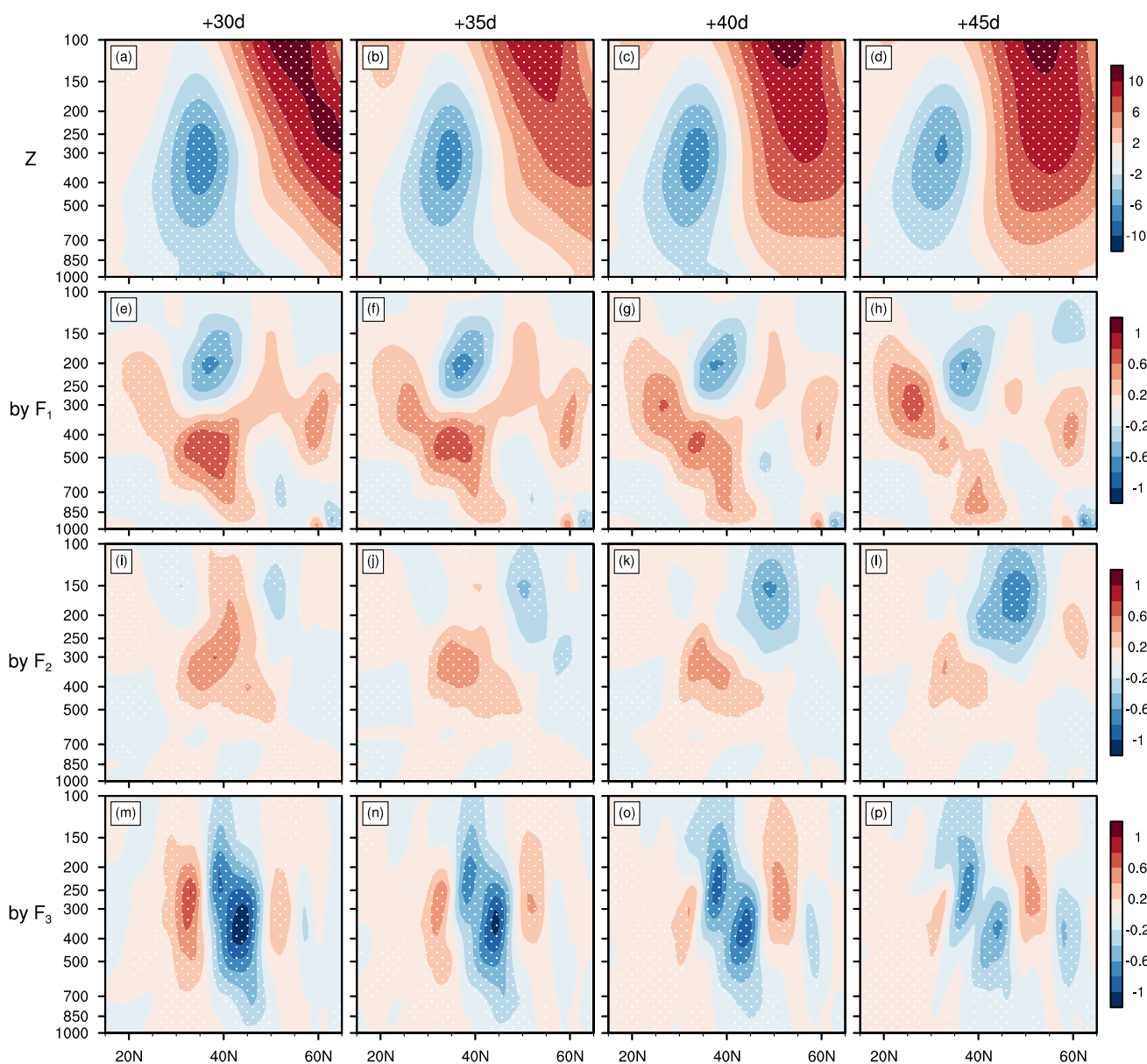
Fig. 7 (continued)

4.3 Ocean–atmosphere interaction processes over the SAFZ

Through the above analysis, it can be seen that the generation and evolution of SAFZ-SST variability during the wintertime is accompanied with clear local ocean–atmosphere interaction processes. The initial anticyclonic surface wind anomaly associated with the weakened AL forces a large-scale warm SST anomaly in midlatitude North Pacific by increasing downward heat flux and driving northward Ekman flow. With the increase of SST anomaly, the direction of air-sea heat flux exchange reverses and the ocean starts to heat the atmosphere. Meanwhile, the warm SST anomaly increases the SST gradient in the north part of SAFZ. The upward THF anomaly helps to synchronize the change of low-level atmospheric baroclinicity to that of the SAFZ, and the transient eddy activities are changed correspondingly. Though all the ocean-induced diabatic heating, transient eddy heating and transient eddy vorticity forcing are enhanced over SAFZ, the last physical process plays the most important role in shifting and maintaining the equivalent barotropic atmospheric circulation anomalies. Our study also provides observational evidence for the unstable ocean–atmosphere interaction mechanism in middle latitudes proposed by Fang and Yang (2016).
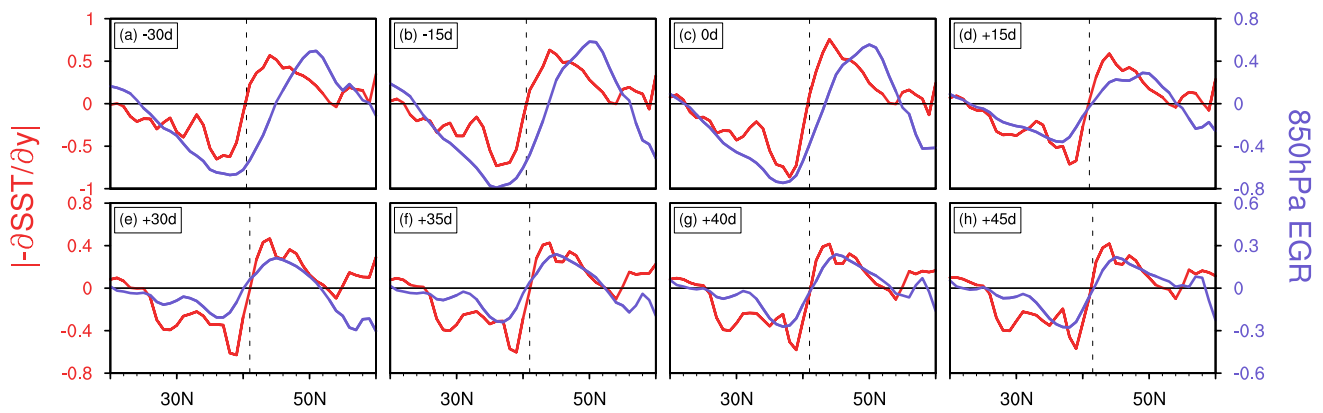
Fig. 8 Lead-lag regression of meridional SST gradient (10^{-6} ℃/m; red line) and EGR at 850 hPa (10^{-5} s^{-1}; violet line) onto the SAFZ-SST index, which are averaged between 144–172°E and 150°E–170°W, respectively. Values exceed 0.05 signifies statistical significance at the 95% confidence level based on the two-tailed Student's t test, and the dashed line marks the center of SAFZ

5 Conclusions and discussion

Different from the thermal-driven tropical atmosphere, the midlatitude atmospheric circulation is generally thermal- and transient eddy-driven. On time-mean scale, the atmospheric forcing sources include direct diabatic heating and indirect transient eddy thermal and dynamical forcing. Recent research works have indicated that the midlatitude oceanic frontal zones are the key regions of ocean–atmosphere interaction. The thermal condition of midlatitude ocean in frontal zones can affect the atmosphere efficiently by changing both the diabatic heating and the transient eddy feedback (Nakamura et al. 2004; Taguchi et al. 2012; Fang and Yang 2016; Tao et al. 2020).

In the North Pacific, a mechanism of unstable ocean–atmosphere interaction associated with the STFZ is proposed to explain the development and maintenance of the PDO-related atmospheric anomalies (Fang and Yang 2016). In this study, we further investigate the SAFZ-related SST variability and the corresponding anomalies of ocean–atmosphere system in winter. The associated ocean–atmosphere interaction processes and their roles in the development and evolution of the air-sea anomalies are examined through observational and theoretical analyses.

The SST variability in SAFZ shows a large-scale pattern with a warming anomaly in the western-to-central midlatitude North Pacific and a surrounding cooling anomaly in its positive phase. It is an interannual midlatitude oceanic mode of the North Pacific that is independent of ENSO. Lead-lag regression analysis illustrates that the SST anomaly can persist during the whole winter season, and its corresponding atmospheric circulation anomalies display a strong positive SLP anomaly (weakened AL) to the north of 40°N and a

week negative SLP anomaly in its south in the leading phase. The positive anomaly peaks at about − 15 day, then decays rapidly and retreats to the north, while the negative SLP anomaly is enhanced and moves northward in the lagging phase. The dipole-type SLP anomaly is reinforced again at + 45 day and then lasts in the rest of winter. Similar characteristics can be also found in the evolution of Z anomalies at different levels, appearing an equivalent barotropic structure in the vertical direction.

Based on the diagnoses of the oceanic mixed-layer temperature tendency equation and the atmospheric QGPV equation, it can be found that the wintertime evolution of SAFZ-related oceanic and atmospheric anomalies is accompanied with local ocean–atmosphere interaction processes. In the leading phase, the anticyclonic surface wind anomaly associated with the weakened AL drives downward heat flux and northward Ekman flow anomalies, leading to a large-scale warm SST anomaly in midlatitude North Pacific. During this time, both the diabatic heating and the transient eddy activities are dominated by the atmosphere. The thermal forcing including diabatic heating and transient eddy heating dominate the total atmospheric forcing and significantly decay the initial atmospheric circulation anomalies.

With the increase of SST anomaly, the heat flux exchange at air-sea interface reverses in the lagging phase, indicating that the ocean starts to heat the atmosphere. In addition to increasing the diabatic heating, the warm SST anomaly strengthens the SST gradient in the north part of SAFZ, and the upward THF anomaly helps to synchronize the change of low-level atmospheric baroclinicity to that of the SAFZ. As a result, the transient eddy heating and transient eddy vorticity forcing are both enhanced over SAFZ. Mainly forced by the transient eddy vorticity forcing, the equivalent barotropic
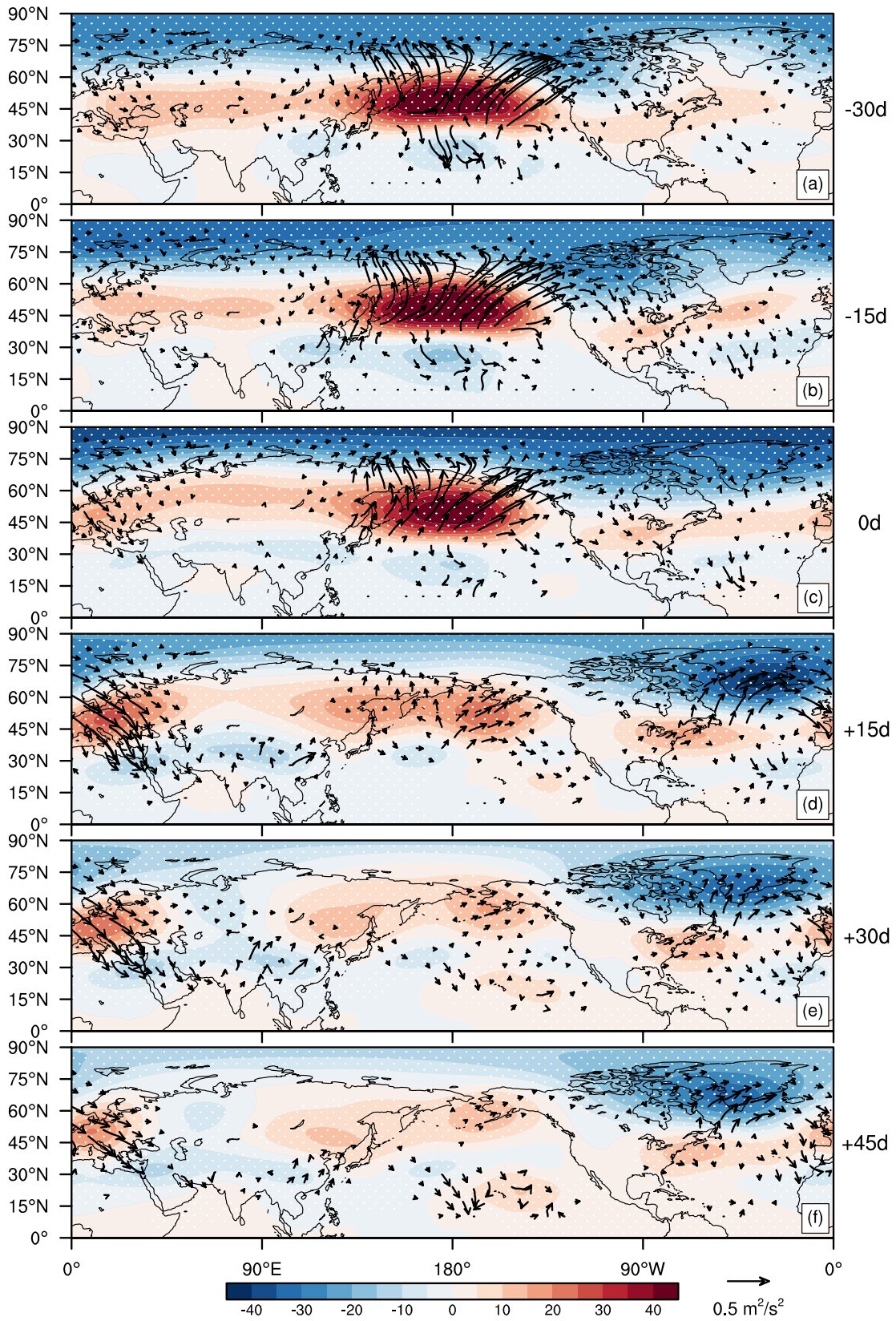
Z200 and T-N WAF

atmospheric circulation anomalies maintain and slightly shift northward.

Therefore, during the processes of air-sea interaction, the atmosphere forces the ocean in the leading phase while the ocean turns to force the atmosphere in the lagging phase. Although compared with the atmospheric forcing on the ocean, the feedback of the ocean is weak and requires a relatively long time for adjustment (nearly 1 month), it can still be clearly identified in the observation. It is the feedback effect of the ocean on the atmosphere that enables the atmospheric anomalies to be maintained throughout the winter, and even has a cross-seasonal impact on the downstream and subtropical regions. Our study further provides observational evidence for the unstable ocean–atmosphere interaction mechanism in middle latitudes proposed by Fang and Yang (2016).

Our study mainly focuses on the local ocean–atmosphere interaction processes associated with SAFZ-SST variability in the North Pacific basin, but issues like what causes the initial AL anomaly and how about the potential influence of local system on the surrounding regions, still need further discussion. As a tentative exploration, we analyze the anomalous 200 hPa Z and the T-N wave activity flux (T-N WAF) (Takaya and Nakamura 2001) in the Northern Hemisphere (Fig. 9). The initial atmospheric circulation anomaly exhibits a large-scale pattern of the positive phase of Arctic Oscillation (AO). The positive Z anomaly is strongest in the North Pacific, corresponding to the weakened AL. In the leading phase, the correlated wave energies are largely dispersed from the AL center into the North America, Arctic region and subtropical North Pacific (Fig. 9a–c), demonstrating potential influence from the North Pacific ocean–atmosphere system to downstream and Arctic region. It is also found that the anomalous center of atmospheric circulation shifts to the North Atlantic region in the lagging phase, transitioning from the positive phase of AO into the positive phase of North Atlantic Oscillation (NAO) (Fig. 9d–f), consistent with the finding of Zhang et al. (2020). The local ocean–atmosphere interaction associated with SAFZ provides energy support for the atmospheric anomaly in the North Pacific and its impact on the downstream and subtropical regions. More research based on observation and numerical experiments will be carried out to verify the mechanism of ocean–atmosphere interaction in the midlatitude North

Pacific and its connection with the Arctic and North Atlantic regions.

In addition, our study emphasizes the SAFZ-SST anomaly impacting on the large-scale atmospheric circulation over the North Pacific. However, its potential influence on the storm track and upper jet stream, which is also a prominent climatic phenomenon in the North Pacific, e.g., the "mid-winter activity minimum" of the storm track (Nakamura and Sampe 2002; Nakamura et al. 2004), remains to be further studied. Besides, as the global warming and climate crisis worsen, some insignificant factors in the past may show up and make an impact on the atmospheric circulation, e.g., the anthropogenic factor (Liu and Di Lorenzo 2018). Future study also needs to consider about the influence from climate change.

Appendix

Decomposition of turbulent heat flux

According to the bulk formulas (Yu et al. 2008),

$$SHF \uparrow = \rho C_p c_h U \Delta T, \tag{3}$$

$$LHF \uparrow = \rho L_e c_e U \Delta q, \tag{4}$$

the THF (SHF + LHF) is determined by the near-surface wind speed and the temperature and specific humidity differences between sea surface and near-surface air. In order to quantify the influences of ocean and atmosphere during the evolution process, we further perform the decomposition of SHF and LHF after Wang et al. (2018) as

$$SHF \uparrow = \overline{SHF \uparrow} + SHF \uparrow', \tag{5}$$

$$LHF \uparrow = \overline{LHF \uparrow} + LHF \uparrow', \tag{6}$$

$$SHF \uparrow' = \rho C_p c_h \left[\overline{U} \Delta T' + U' \overline{\Delta T} + \left(U' \Delta T' \right)' \right], \tag{7}$$

$$LHF \uparrow' = \rho L_e c_e \left[\overline{U} \Delta q' + U' \overline{\Delta q} + \left(U' \Delta q' \right)' \right], \tag{8}$$

where the overbar denotes the climatological mean component and the prime denotes the anomalous component. Revealed by Eqs. 6 and 7, the anomaly of SHF and LHF consists of three components: the anomalous sea-air temperature or specific humidity difference-related term $\rho C_p c_h \overline{U} \Delta T'$ (hereafter denoted by S_1) or $\rho L_e c_e \overline{U} \Delta q'$ (L_1), which is affected by both oceanic and atmospheric anomalies; the

anomalous near-surface wind speed-related term $\rho C_p c_h U' \overline{\Delta T}$ (S_2) or $\rho L_e c_e U' \overline{\Delta q}$ (L_2), which is only affected by the atmospheric anomaly; and the anomaly of nonlinear interaction term $\rho C_p c_h \left(U' \Delta T' \right)'$ (S_3) or $\rho L_e c_e \left(U' \Delta q' \right)'$ (L_3).

However, the anomalous sea-air difference-related term still contains the influences both by ocean and atmosphere, so we further decompose the term $\rho C_p c_h \overline{U} \Delta T'$ and $\rho L_e c_e \overline{U} \Delta q'$ into

$$\rho C_p c_h \overline{U} \Delta T' = \rho C_p c_h \overline{U} T'_s - \rho C_p c_h \overline{U} T'_a, \tag{9}$$

$$\rho L_e c_e \overline{U} \Delta q' = \rho L_e c_e \overline{U} q'_s - \rho L_e c_e \overline{U} q'_a, \tag{10}$$

where T_s and T_a are the respective sea surface and near-surface air temperatures, q_s and q_a the respective sea surface and near-surface atmospheric specific humidity. Now that the oceanic and atmospheric influences are well separated, we could quantitatively diagnose their contributions to THF during the interaction process.

The results are shown in Fig. 10. Consistent with the evolution in Fig. 3, the transition of THF anomaly occurs

after SST anomaly reaching its maximum. In the leading phase, the SHF anomaly is determined by both the anomalous sea-air temperature difference-related term (S_1) and the anomalous near-surface wind speed-related term (S_2), while the LHF anomaly is only dominated by the anomalous near-surface wind speed-related term (L_2) (Fig. 10a, c). Detailed decomposition of S_1 suggests the ocean (atmosphere) always tends to induce upward (downward) heat flux anomaly, but the contribution of the atmosphere exceeds that of the ocean at this time (Fig. 10b). Hence it is the atmosphere that dominates the downward heat flux anomaly in the leading phase. When it comes to the lagging phase, the SHF and LHF anomaly is only dominated by S_1 and L_1, respectively (Fig. 10a, c). Different from that in the leading phase, S_2 and L_2 are very small because of the rapid weakening of anticyclone anomaly and its accompanied wind anomaly. And the detailed decomposition of S_1 and L_1 further suggests the ocean indeed dominates in the lagging phase (Fig. 10b, d). Therefore, the reversal of THF anomaly reflects the feedback of the ocean on the atmosphere in the lagging phase.
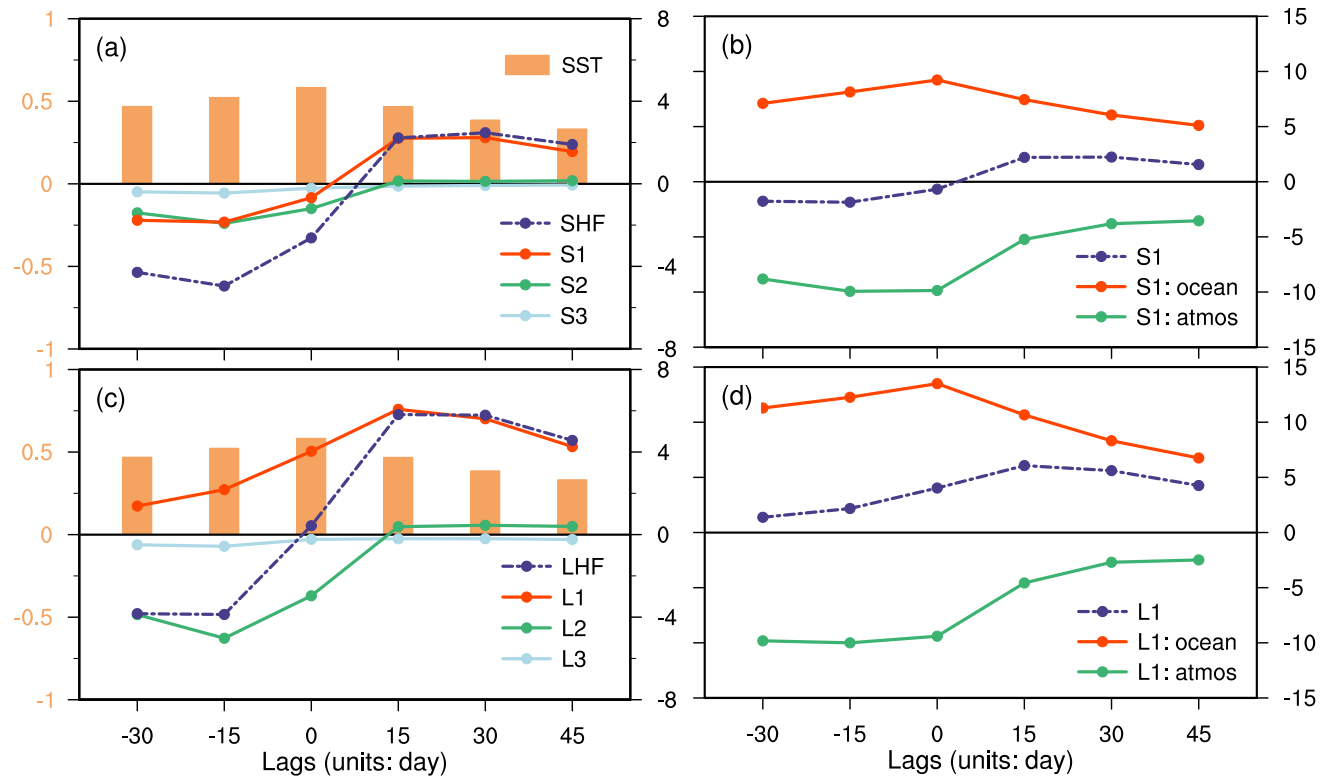

Fig. 10 Lead-lag regression of **a** SHF, **b** S_1, **c** LHF and **d** L_1 (dark violet line) and their terms of decomposition (W/m²) onto the SAFZ-SST index, which are averaged in the SAFZ region (i.e., 37.5°–44.5°N, 144°–172°E). In **a** and **c**, red line denotes the anomalous sea-air temperature or specific humidity difference-related term (S_1 or L_1), green line the anomalous near-surface wind speed-related term (S_2 or L_2), and light blue line the anomaly of nonlinear interaction term (S_3 or L_3). Regressed SST (℃) is indicated by the orange bar. In **b** and **d**, red line represents the contribution from ocean, and green line from atmosphere

Declarations

References

Bretherton CS, Widmann M, Dymnikov VP, Wallace JM, Blade I (1999) The effective number of spatial degrees of freedom of a time-varying field. J Clim 12:1990–2009. https://doi.org/10.1175/1520-0442(1999)012%3c1990:Tenosd%3e2.0.Co;2

Carton JA, Chepurin GA, Chen LG (2018) SODA3: a new ocean climate reanalysis. J Clim 31:6967–6983. https://doi.org/10.1175/jcli-d-18-0149.1

Chang EKM, Orlanski I (1993) On the dynamics of a storm track. J Atmos Sci 50:999–1015. https://doi.org/10.1175/1520-0469(1993)050%3c0999:OTDOAS%3e2.0.CO;2

Chang EKM, Lee S, Swanson K (2002) Storm track dynamics. J Clim 15:2163–2183. https://doi.org/10.1175/1520-0442(2002)015%3c02163:STD%3e2.0.CO;2

Chen L, Fang J, Yang X-Q (2020) Midlatitude unstable air-sea interaction with atmospheric transient eddy dynamical forcing in an analytical coupled model. Clim Dyn 55:2557–2577. https://doi.org/10.1007/s00382-020-05405-0

Christy JR (1991) Diabatic heating rate estimates from European Centre for Medium-Range Weather Forecasts analyses. J Geophys Res Atmos 96:5123–5135. https://doi.org/10.1029/90JD02687

Chu C, Yang X-Q, Ren X, Zhou T (2013) Response of northern hemisphere storm tracks to Indian-western Pacific Ocean warming in atmospheric general circulation models. Clim Dyn 40:1057–1070. https://doi.org/10.1007/s00382-013-1687-y

Czaja A, Blunt N (2011) A new mechanism for ocean-atmosphere coupling in midlatitudes. Q J R Meteorol Soc 137:1095–1101. https://doi.org/10.1002/qj.814

Deser C, Magnusdottir G, Saravanan R, Phillips A (2004) The effects of North Atlantic SST and sea ice anomalies on the winter circulation in CCM3. Part II: direct and indirect components of the response. J Clim 17:877–889. https://doi.org/10.1175/1520-0442(2004)017%3c0877:teanas%3e2.0.co;2

Eady ET (1949) Long waves and cyclone waves. Tellus 1:33–52. https://doi.org/10.3402/tellusa.v1i3.8507

Fang J, Yang X-Q (2016) Structure and dynamics of decadal anomalies in the wintertime midlatitude North Pacific ocean-atmosphere system. Clim Dyn 47:1989–2007. https://doi.org/10.1007/s00382-015-2946-x

Fang J, Chen L, Yang X-Q (2022) Roles of vertical distributions of atmospheric transient eddy dynamical forcing and diabatic heating in midlatitude unstable air–sea interaction. Clim Dyn 58:351–368. https://doi.org/10.1007/s00382-021-05912-8

Feliks Y, Ghil M, Simonnet E (2004) Low-frequency variability in the midlatitude atmosphere induced by an oceanic thermal front. J Atmos Sci 61:961–981. https://doi.org/10.1175/1520-0469(2004)061%3c0961:lvitma%3e2.0.co;2

Feliks Y, Ghil M, Simonnet E (2007) Low-frequency variability in the midlatitude baroclinic atmosphere induced by an oceanic thermal front. J Atmos Sci 64:97–116. https://doi.org/10.1175/jas3780.1

Feliks Y, Ghil M, Robertson AW (2011) The atmospheric circulation over the North Atlantic as induced by the SST field. J Clim 24:522–542. https://doi.org/10.1175/2010jcli3859.1

Frankignoul C, Sennéchael N, Kwon YO, Alexander MA (2011) Influence of the meridional shifts of the Kuroshio and the Oyashio Extensions on the atmospheric circulation. J Clim 24:762–777. https://doi.org/10.1175/2010jcli3731.1

Hasselmann K (1976) Stochastic climate models part i. Theory Tellus 28:473–485. https://doi.org/10.3402/tellusa.v28i6.11316

Hoskins BJ, Valdes PJ (1990) On the existence of storm-tracks. J Atmos Sci 47:1854–1864. https://doi.org/10.1175/1520-0469(1990)047%3c1854:oteost%3e2.0.co;2

Hotta D, Nakamura H (2011) On the significance of the sensible heat supply from the ocean in the maintenance of the mean baroclinicity along storm tracks. J Clim 24:3377–3401. https://doi.org/10.1175/2010jcli3910.1

Kelly KA, Small RJ, Samelson RM, Qiu B, Joyce TM, Kwon YO, Cronin MF (2010) Western boundary currents and frontal air-sea interaction: Gulf Stream and Kuroshio Extension. J Clim 23:5644–5667. https://doi.org/10.1175/2010jcli3346.1

Kushnir Y, Lau N-C (1992) The General Circulation Model response to a North Pacific SST anomaly: dependence on time scale and pattern polarity. J Clim 5:271–283. https://doi.org/10.1175/1520-0442(1992)005%3c0271:tgcmrt%3e2.0.co;2

Kushnir Y, Held IM (1996) Equilibrium atmospheric response to North Atlantic SST anomalies. J Clim 9:1208–1220. https://doi.org/10.1175/1520-0442(1996)009<1208:EARTNA>2.0.CO;2

Kushnir Y, Robinson WA, Bladé I, Hall NMJ, Peng S, Sutton R (2002) Atmospheric GCM response to extratropical SST anomalies: synthesis and evaluation. J Clim 15:2233–2256. https://doi.org/10.1175/1520-0442(2002)015%3c2233:agrtes%3e2.0.co;2

Kwon YO, Alexander MA, Bond NA, Frankignoul C, Nakamura H, Qiu B, Thompson L (2010) Role of the Gulf Stream and Kuroshio-Oyashio systems in large-scale atmosphere-ocean interaction: a review. J Clim 23:3249–3281. https://doi.org/10.1175/2010jcli3343.1

Lau NC, Holopainen EO (1984) Transient eddy forcing of the time-mean flow as identified by geopotential tendencies. J Atmos Sci 41:313–328. https://doi.org/10.1175/1520-0469(1984)041%3c0313:Tefott%3e2.0.Co;2

Lindzen RS, Farrell B (1980) A simple approximate result for the maximum growth rate of baroclinic instabilities. J Atmos Sci 37:1648–1654. https://doi.org/10.1175/1520-0469(1980)037%3c1648:asarft%3e2.0.co;2

Liu ZY, Di Lorenzo E (2018) Mechanisms and predictability of Pacific decadal variability. Curr Clim Change Rep 4:128–144. https://doi.org/10.1007/s40641-018-0090-5

Liu C, Ren X, Yang X-Q (2014) Mean flow-storm track relationship and Rossby wave breaking in two types of El-Niño. Adv Atmos Sci 31:197–210. https://doi.org/10.1007/s00376-013-2297-7

Minobe S, Kuwano-Yoshida A, Komori N, Xie S-P, Small RJ (2008) Influence of the Gulf Stream on the troposphere. Nature 452:206–209. https://doi.org/10.1038/nature06690

Nakamura H, Kazmin AS (2003) Decadal changes in the North Pacific oceanic frontal zones as revealed in ship and satellite observations. J Geophys Res. https://doi.org/10.1029/1999jc000085

Nakamura H, Sampe T (2002) Trapping of synoptic-scale disturbances into the north-Pacific subtropical jet core in midwinter. Geophys Res Lett 29:8-1–8-4. https://doi.org/10.1029/2002GL015535

Nakamura H, Shimpo A (2004) Seasonal variations in the Southern Hemisphere storm tracks and jet streams as revealed in a reanalysis dataset. J Clim 17:1828–1844. https://doi.org/10.1175/1520-0442(2004)017%3c1828:Svitsh%3e2.0.Co;2

Nakamura H, Yamagata T (1999) Recent decadal SST variability in the northwestern Pacific and associated atmospheric anomalies. In: Navarra A (ed) Beyond El Niño: decadal and interdecadal climate variability. Springer, Berlin, Heidelberg, pp 49–72

Nakamura M, Yamane S (2009) Dominant anomaly patterns in the near-surface baroclinicity and accompanying anomalies in the atmosphere and oceans. Part I: North Atlantic basin. J Clim 22:880–904. https://doi.org/10.1175/2008jcli2297.1

Nakamura M, Yamane S (2010) Dominant anomaly patterns in the near-surface baroclinicity and accompanying anomalies in the atmosphere and oceans. Part II: North Pacific basin. J Clim 23:6445–6467. https://doi.org/10.1175/2010jcli3017.1

Nakamura H, Lin G, Yamagata T (1997) Decadal climate variability in the North Pacific during the recent decades. Bull Am Meteor Soc 78:2215–2225. https://doi.org/10.1175/1520-0477(1997)078%3c2215:DCVITN%3e2.0.CO;2

Nakamura H, Sampe T, Tanimoto Y, Shimpo A (2004) Observed associations among storm tracks, jet streams and midlatitude oceanic fronts. In: Wang C, Xie S-P, Carton JA (eds) Earth's climate: the ocean-atmosphere interaction, 1st edn. American Geophysical Union, Washington, pp 329–345

Nakamura H, Sampe T, Goto A, Ohfuchi W, Xie S-P (2008) On the importance of midlatitude oceanic frontal zones for the mean state and dominant variability in the tropospheric circulation. Geophys Res Lett. https://doi.org/10.1029/2008gl034010

Nie Y, Zhang Y, Yang X-Q, Chen G (2013) Baroclinic anomalies associated with the Southern Hemisphere Annular Mode: roles of synoptic and low-frequency eddies. Geophys Res Lett 40:2361–2366. https://doi.org/10.1002/grl.50396

Nie Y, Zhang Y, Chen G, Yang X-Q, Burrows DA (2014) Quantifying barotropic and baroclinic eddy feedbacks in the persistence of the Southern Annular Mode. Geophys Res Lett 41:8636–8644. https://doi.org/10.1002/2014gl062210

Nonaka M, Nakamura H, Tanimoto Y, Kagimoto T, Sasaki H (2006) Decadal variability in the Kuroshio-Oyashio Extension simulated in an eddy-resolving OGCM. J Clim. https://doi.org/10.1175/JCLI3793.1

Nonaka M, Nakamura H, Tanimoto Y, Kagimoto T, Sasaki H (2008) Interannual-to-decadal variability in the Oyashio and its influence on temperature in the subarctic frontal zone: an eddy-resolving OGCM simulation. J Clim 21:6283–6303. https://doi.org/10.1175/2008jcli2294.1

Nonaka M, Nakamura H, Taguchi B, Komori N, Kuwano-Yoshida A, Takaya K (2009) Air-sea heat exchanges characteristic of a prominent midlatitude oceanic front in the south Indian Ocean as simulated in a high-resolution coupled GCM. J Clim 22:6515–6535. https://doi.org/10.1175/2009JCLI2960.1

Okajima S, Nakamura H, Kaspi Y (2022) Energetics of transient eddies related to the midwinter minimum of the North Pacific storm-track activity. J Clim 35:1137–1156. https://doi.org/10.1175/jcli-d-21-0123.1

Palmer TN, Sun Z (1985) A modelling and observational study of the relationship between sea surface temperature in the north-west Atlantic and the atmospheric general circulation. Q J R Meteorol Soc 111:947–975. https://doi.org/10.1002/qj.49711147003

Pierce DW, Barnett TP, Schneider N, Saravanan R, Dommenget D, Latif M (2001) The role of ocean dynamics in producing decadal climate variability in the North Pacific. Clim Dyn 18:51–70. https://doi.org/10.1007/s003820100158

Qiu B (2000) Interannual variability of the Kuroshio Extension system and its impact on the wintertime SST field. J Phys Oceanogr 30:1486–1502. https://doi.org/10.1175/1520-0485(2000)030%3c1486:ivotke%3e2.0.co;2

Qiu B, Chen SM, Schneider N, Taguchi B (2014) A coupled decadal prediction of the dynamic state of the Kuroshio Extension system. J Clim 27:1751–1764. https://doi.org/10.1175/jcli-d-13-00318.1

Ren X, Yang X-Q, Han B, Xu G (2007) North Pacific storm track variations in winter season and the coupled pattern with the midlatitude atmosphere-ocean system. Chin J Geophys 50:94–103. https://doi.org/10.1002/cjg2.1014

Ren X, Yang X-Q, Chu C (2010) Seasonal variations of the synoptic-scale transient eddy activity and polar front jet over east Asia. J Clim 23:3222–3233. https://doi.org/10.1175/2009jcli3225.1

Sampe T, Nakamura H, Goto A, Ohfuchi W (2010) Significance of a midlatitude SST frontal zone in the formation of a storm track and an eddy-driven westerly jet. J Clim 23:1793–1814. https://doi.org/10.1175/2009jcli3163.1

Seager R, Kushnir Y, Henderson N, Cane M, Miller J (2001) Wind-driven shifts in the latitude of the Kuroshio-Oyashio Extension and generation of SST anomalies on decadal timescales. J Clim 14:4249–4265. https://doi.org/10.1175/1520-0442(2001)014%3c4249:WDSITL%3e2.0.CO;2

Small RJ, deSzoeke SP, Xie S-P, O'Neill L, Seo H, Song Q et al (2008) Air–sea interaction over ocean fronts and eddies. Dyn Atmos Oceans 45:274–319. https://doi.org/10.1016/j.dynatmoce.2008.01.001

Smirnov D, Newman M, Alexander MA, Kwon Y-O, Frankignoul C (2015) Investigating the local atmospheric response to a realistic shift in the Oyashio sea surface temperature front. J Clim 28:1126–1147. https://doi.org/10.1175/jcli-d-14-00285.1

Sun X, Tao L, Yang X-Q (2018) The influence of oceanic stochastic forcing on the atmospheric response to midlatitude North Pacific SST anomalies. Geophys Res Lett 45:9297–9304. https://doi.org/10.1029/2018gl078860

Taguchi B, Nakamura H, Nonaka M, Xie S-P (2009) Influences of the Kuroshio/Oyashio Extensions on air-sea heat exchanges and storm-track activity as revealed in regional atmospheric model simulations for the 2003/04 cold season. J Clim 22:6536–6560. https://doi.org/10.1175/2009jcli2910.1

Taguchi B, Nakamura H, Nonaka M, Komori N, Kuwano-Yoshida A, Takaya K, Goto A (2012) Seasonal evolutions of atmospheric response to decadal SST anomalies in the North Pacific subarctic frontal zone: observations and a coupled model simulation. J Clim 25:111–139. https://doi.org/10.1175/jcli-d-11-00046.1

Takaya K, Nakamura H (2001) A formulation of a phase-independent wave-activity flux for stationary and migratory quasigeostrophic eddies on a zonally varying basic flow. J Atmos Sci 58:608–627. https://doi.org/10.1175/1520-0469(2001)058%3c0608:AFOAPI%3e2.0.CO;2

Tao L, Yang X-Q, Fang J, Sun X (2020) PDO-related wintertime atmospheric anomalies over the midlatitude North Pacific: local versus remote SST forcing. J Clim. https://doi.org/10.1175/JCLI-D-19-0143.1

Tao L, Fang J, Yang X-Q, Sun X, Cai D (2022) Midwinter reversal of the atmospheric anomalies caused by the North Pacific Mode-related air-sea coupling. Geophys Res Lett. https://doi.org/10.1029/2022gl100307

Wang L, Yang X-Q, Yang D, Xie Q, Fang J, Sun X (2017) Two typical modes in the variabilities of wintertime North Pacific basin-scale oceanic fronts and associated atmospheric eddy-driven jet. Atmos Sci Lett 18:373–380. https://doi.org/10.1002/asl.766

Wang T, Yang X-Q, Fang J, Sun X, Ren X (2018) Role of air–sea interaction in the 30–60-day boreal summer intraseasonal oscillation over the western North Pacific. J Clim 31:1653–1680. https://doi.org/10.1175/jcli-d-17-0109.1

Wills SM, Thompson DWJ (2018) On the observed relationships between wintertime variability in Kuroshio-Oyashio Extension sea surface temperatures and the atmospheric circulation over the North Pacific. J Clim 31:4669–4681. https://doi.org/10.1175/jcli-d-17-0343.1

Xiang Y, Yang X-Q (2012) The effect of transient eddy on interannual meridional displacement of summer east Asian subtropical jet. Adv Atmos Sci 29:484–492. https://doi.org/10.1007/s00376-011-1113-5

Yanai M, Tomita T (1998) Seasonal and interannual variability of atmospheric heat sources and moisture sinks as determined from ncep-ncar reanalysis. J Clim 11:463–482. https://doi.org/10.1175/1520-0442(1998)011%3c0463:saivoa%3e2.0.co;2

Yao Y, Zhong Z, Yang X-Q, Lu W (2017) An observational study of the North Pacific storm-track impact on the midlatitude oceanic front. J Gerontol Ser A Biol Med Sci 122:6962–6975. https://doi.org/10.1002/2016jd026192

Yao Y, Zhong Z, Yang XQ (2018) Impacts of the subarctic frontal zone on the North Pacific storm track in the cold season: an observational study. Int J Climatol 38:2554–2564. https://doi.org/10.1002/joc.5429

Yook S, Thompson DWJ, Sun L, Patrizio CR (2022) The simulated atmospheric response to western North Pacific sea-surface temperature anomalies. J Clim. https://doi.org/10.1175/jcli-d-21-0371.1

Yu L, Jin X, Weller R (2008) Multidecade global flux datasets from the objectively analyzed air–sea fluxes (OAFlux) project: latent and sensible heat fluxes, ocean evaporation, and related surface meteorological variables. OAFlux Project Tech. Rep. OA-2008-01. https://www.researchgate.net/publication/237440650_Multidecade_Global_Flux_Datasets_from_the_Objectively_Analyzed_Air-sea_Fluxes_OAFlux_Project_Latent_and_Sensible_Heat_Fluxes_Ocean_Evaporation_and_Related_Surface_Meteorological_Variables

Zhang L-L, Yang X-Q, Xie Q, Fang J-B (2012) Global atmospheric seasonal-mean heating: diabatic versus transient heating. J Trop Meteorol 18:494–502

Zhang R, Fang J, Yang X-Q (2020) What kinds of atmospheric anomalies drive wintertime North Pacific basin-scale subtropical oceanic front intensity variation? J Clim 33:7011–7026. https://doi.org/10.1175/jcli-d-19-0973.1

Zhong Y, Liu Z, Jacob R (2008) Origin of Pacific multidecadal variability in community climate system model, version 3 (CCSM3): a combined statistical and dynamical assessment. J Clim 21:114–133. https://doi.org/10.1175/2007jcli1730.1